Top-Quark Physics at the LHC

Sven-Olaf Moch[1], *Jürgen Reuter*[2]

[1]II. Institut für Theoretische Physik, Universität Hamburg, Germany
[2]DESY, Hamburg, Germany

DOI: http://dx.doi.org/10.3204/PUBDB-2018-00782/B11

We report on the precision determination of the top-quark mass to next-to-next-to-leading order in QCD in well-defined renormalization schemes using data from the Large Hadron Collider for single-top and top-quark pair production. We also discuss the calibration of the so-called Monte Carlo top-quark mass parameter which is determined from a comparison to events with top-quark decay products. The implications of the measured value of the top-quark mass for conclusions about the stability of the electroweak vacuum state of our Universe are illustrated. At future lepton colliders, we provide for the first time matched exclusive calculations valid both at the top threshold and in the continuum, also fully differentially. In addition, we calculate fully off-shell top-pair production (also with an associated Higgs boson) at next-to-leading order in QCD, which allows to extract the top-Yukawa coupling with an unprecedented precision.

1 Introduction

Top-quark production features among the processes with the largest cross sections at the Large Hadron Collider (LHC). So far, the LHC has collected high quality data at collision energies up to $\sqrt{s} = 13$ TeV to be confronted with the high precision theory predictions of the Standard Model (SM) of particle physics. For the latter, the current state-of-art is based on the Quantum Chromodynamics (QCD) corrections up to the next-to-next-to-leading order (NNLO) in the strong coupling constant α_s, which can be used to determine the top-quark mass m_t at this theoretical accuracy. After the confirmation of the Higgs boson's existence, these measured values of the SM parameters m_t and α_s play a decisive role in addressing questions currently in focus of the scientific community and related to the Higgs boson's implications for our Universe at very early times and the stability of the electroweak vacuum. Altogether this makes top-quark physics at the moment one of the most interesting areas in particle physics and precision predictions for processes at present and future colliders are a necessary prerequisites.

In this article we begin with a brief review of the present theory predictions for the production of single top-quarks and top-quark pairs at the LHC. Then we report on the precision determination of the top-quark mass $m_t(\mu_r)$ to NNLO in QCD in the $\overline{\rm MS}$ scheme at a chosen renormalization scale μ_r from measured cross sections at various center-of-mass energies at the LHC. Related, we also discuss the procedure for the calibration of the Monte Carlo top-quark mass parameter used in the kinematic reconstruction of events with top-quark decay products. Finally, we apply the measured values of m_t and α_s together with their present uncertainties to the running of the Higgs boson's self-coupling at large scales, which indicates stability of the ground state of the electroweak theory.

	$\sqrt{s} = 7$ TeV	$\sqrt{s} = 8$ TeV	$\sqrt{s} = 13$ TeV
$\sigma_{pp\to t\bar{t}}$ [pb]	$171.8^{+0.1}_{-5.3} \pm 3.4$	$247.5^{+0.0}_{-7.5} \pm 4.6$	$831.4^{+0.0}_{-23.1} \pm 14.5$

Table 1: Cross section for top-quark pair production at NNLO in QCD with errors shown as $\sigma + \Delta\sigma_{\rm scale} + \Delta\sigma_{\rm PDF}$ at various center-of-mass energies of the LHC using $m_t(m_t) = 160.9$ GeV in the $\overline{\rm MS}$ scheme and the ABMP16 PDF set [1]. The scale uncertainty $\Delta\sigma_{\rm scale}$ is based on the shifts for the choices $\mu_r = \mu_f = m_t(m_t)/2$ and $\mu_r = \mu_f = 2m_t(m_t)$ and $\Delta\sigma_{\rm PDF}$ is the 1σ combined PDF+α_s+m_t error.

At future electron-positron colliders, such as the planned International Linear Collider (ILC), the top-quarks can be copiously produced by operating at center-of-mass energies around the threshold to top-quark pair production. With the large statistics collected under such conditions and the significantly reduced uncertainties due to experimental systematics in collisions with electrons and positrons, the ILC is ideally suited for an improved precision measurement of m_t as well as for investigating possible deviations from SM predictions in the top-quark related processes. These aspects are detailed in the final section of this article.

2 Top-quark physics at the LHC

2.1 Inclusive top-quark hadro-production

The theoretical description of both top-quark pair production and single-top production has reached a very high level of accuracy. According to the standard QCD factorization the cross section is given as

$$\sigma_{pp\to X}(s, m_t^2) = \sum_{ij} f_i(\mu_f^2) \otimes f_j(\mu_f^2) \otimes \hat{\sigma}_{ij\to X}\left(\alpha_s(\mu_r), s, m_t^2, \mu_f^2\right) \ , \tag{1}$$

where μ_f and μ_r are the factorization and renormalization scale and s is the center-of-mass energy. The parton distribution functions (PDFs) in the proton are denoted by f_i $(i = q, \bar{q}, g)$ and $\hat{\sigma}_{ij\to X}$ is the (hard) subprocess cross section for parton types i and j to produce the final state X, which can be a single top-quark or a $t\bar{t}$ pair. Both, PDFs and the partonic cross sections in Eq. (1) are subject to the standard convolution in the parton momentum fractions, denoted as "$\otimes$". The top-quark mass in Eq. (1) requires the choice of a renormalization scheme, which we take to be the $\overline{\rm MS}$ scheme, that is using $m_t(\mu_r)$.

The hadro-production of $t\bar{t}$ pairs is a QCD process at Born level, i.e., the leading order contributions to $\hat{\sigma}_{ij\to t\bar{t}}$ are proportional to α_s^2 and the gluon-gluon-fusion process $gg \to t\bar{t}$ driven by the gluon PDF dominates. Higher order corrections to the respective inclusive partonic cross sections have been calculated up to the NNLO in perturbative QCD [2–5] and the result shows good apparent convergence of the perturbative expansion and greatly reduced sensitivity with respect to variations of the scales μ_r and μ_f. The latter is conventionally taken as an estimate of the residual theoretical uncertainty.

In Tab. 1 we quote results for the inclusive $t\bar{t}$ cross section at NNLO accuracy in QCD using the `Hathor` code [6] with the PDF set ABMP16 [1] for various center-of-mass energies of the LHC, $\sqrt{s} = 7, 8$, and 13 TeV. The top-quark mass taken in the $\overline{\rm MS}$ scheme is set to

$m_t(m_t) = 160.9$ GeV and the strong coupling to $\alpha_s^{(n_f=5)}(M_Z) = 0.1147$. The PDF uncertainties quoted represent the combined symmetric 1σ uncertainty $\Delta\sigma(\text{PDF} + \alpha_s + m_t)$ arising from the variation of the PDF parameters, α_s and m_t in 29 PDF sets of ABMP16. Thanks to the high precision LHC data used in the ABMP16 fit and NNLO accuracy in QCD the overall cross section uncertainty is significantly reduced.

Single-top production on the other hand generates the top-quark in an electroweak interaction at Born level. This proceeds predominantly in a vertex with a W-boson, top- and bottom-quark and its orientation assigns single-top production diagrams to different channels. At the LHC, the t-channel process (Fig. 1b) dominates, while the cross section for Wt-production (Fig. 1c) is typically smaller by one order of magnitude and the s-channel contribution (Fig. 1a) is negligible.

Higher order QCD corrections to the inclusive parton cross sections $\hat{\sigma}_{ij\to t}$ for the single-top production in the t-channel are known to NNLO in the so-called structure function approximation [7] (see also Ref. [8]), which separately accounts for the QCD corrections to the light- and heavy-quark lines, see Fig. 1b, neglecting dynamical cross-talk between the two quark lines, which is expected to be small due to color suppression. Moreover, the known NNLO QCD corrections to $\hat{\sigma}_{ij\to t}$ are quite small. For the inclusive cross section Ref. [7] has reported the ratios $\sigma^{\text{NNLO}}_{pp\to t}/\sigma^{\text{NLO}}_{pp\to t} \simeq -1.6\%$ and $\sigma^{\text{NNLO}}_{pp\to \bar{t}}/\sigma^{\text{NLO}}_{pp\to \bar{t}} \simeq -1.3\%$ at $\sqrt{s} = 8$ TeV for a pole mass $m_t^{\text{pole}} = 173.2$ GeV.

The cross sections for t-channel single-top production are directly proportional to the light quark PDFs. These are nowadays well constrained by data on the measured charged lepton asymmetries from $W^{\pm}$ gauge-boson production at the LHC [9]. Therefore data on cross sections for t-channel production of single top-quarks offers the interesting possibility for a determination of m_t, which is not subject to strong correlations between m_t, α_s and the gluon PDF as is the case for the cross section for $t\bar{t}$-pair production.

In Figs. 2 and 3 we display the cross sections $\sigma_{pp\to\bar{t}}$ and $\sigma_{pp\to\bar{t}}$ at next-to-leading order (NLO) in QCD (computed with the `Hathor` library [6, 10]) for LHC energies of $\sqrt{s} = 7$ and 8 TeV, respectively, using $m_t(m_t) = 160.9$ GeV with scale choice $\mu_r = \mu_f = m_t(m_t)$ and compare with data from ATLAS [11] and CMS [12]. We use the NNLO PDF sets of ABMP16 [1]. CT14 [13], MMHT14 [14], and NNPDF3.1 [15] and central value for each PDF set is complemented by the symmetrized PDF uncertainty. Within the current large experimental uncertainties all predictions in Figs. 2 and 3 agree with the data.

In the ratio of the cross sections $R_t = \sigma_{pp\to\bar{t}}/\sigma_{pp\to\bar{t}}$ on the other hand many theoretical and experimental uncertainties cancel as shown in Fig. 4. This quantity is thus a very sensitive probe for the ratio of d/u quark PDFs at large x. While still all predictions for R_t with the various PDF sets agree with the data there are systematic shifts visible so that with improved statistics for single-top production at $\sqrt{s} = 13$ TeV, this reaction might serve as a standard candle process in the future, cf. Ref. [9].

2.2 Top-quark mass determination

The available high precision theory predictions for the inclusive top-quark hadro-production can be used to extract the top-quark mass when confronted with accurate measurements of those cross sections at the LHC. See, e.g., Ref. [1] for a recent compilation of the respective LHC data sets and Ref. [17] for a review of earlier work on precise heavy-quark mass determinations, including charm and bottom.

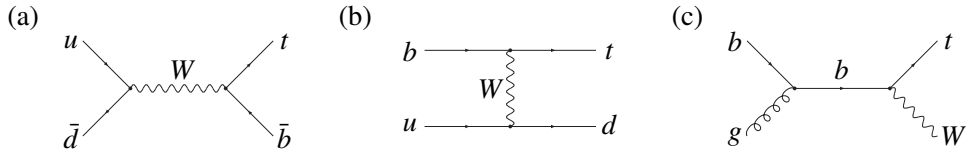

Figure 1: Representative leading order Feynman diagrams for single top-quark production: (a) s-channel; (b) t-channel; (c) in association with a W boson. Figures taken from Ref. [16].

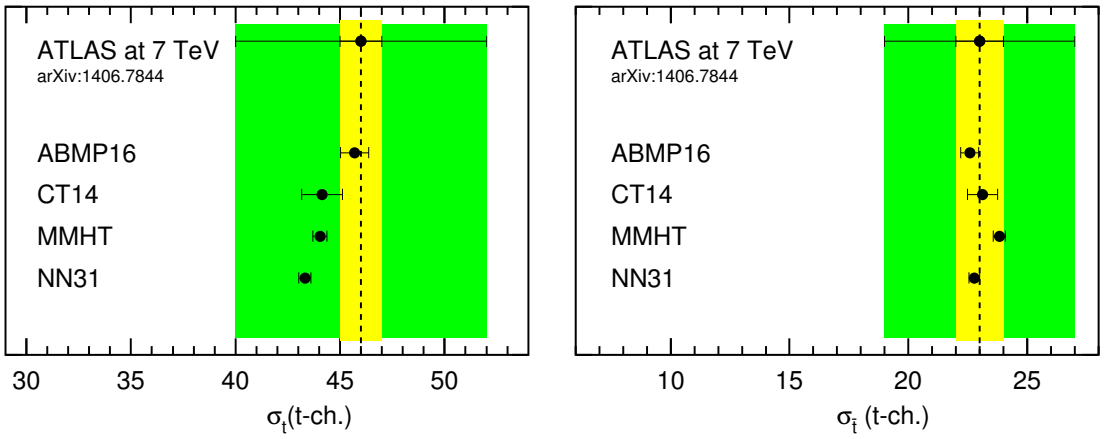

Figure 2: Cross sections together with their 1σ PDF uncertainties for the t-channel production of single (anti)top-quarks in pp collision at $\sqrt{s} = 7$ TeV in comparison to ATLAS data [11] for a $\overline{\text{MS}}$ mass $m_t(m_t) = 160.9$ GeV at the scale $\mu_r = \mu_f = m_t(m_t)$ with PDF sets are taken at NNLO. The inner (yellow) band denotes the statistical uncertainty and the outer (green) band the combined uncertainty due to statistics and systematics.

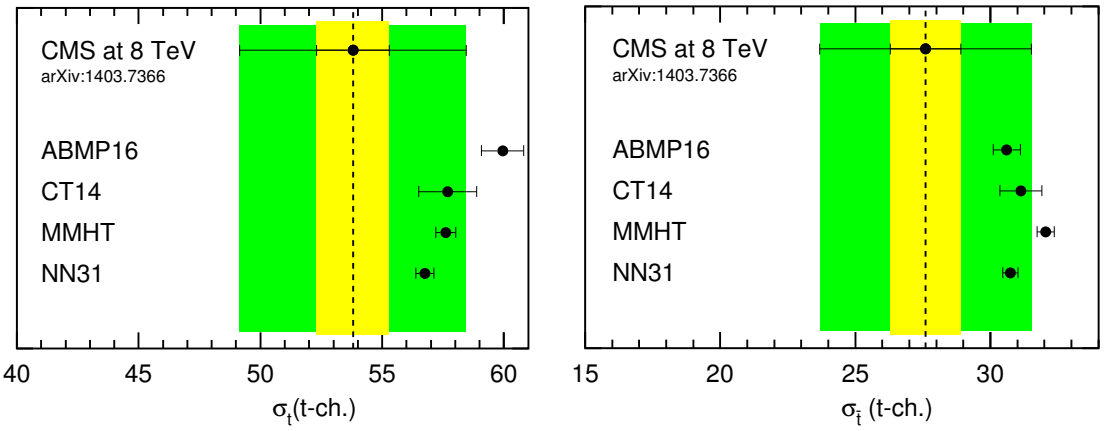

Figure 3: Same as Fig. 2 for pp collision at $\sqrt{s} = 8$ TeV in comparison to CMS data [12].

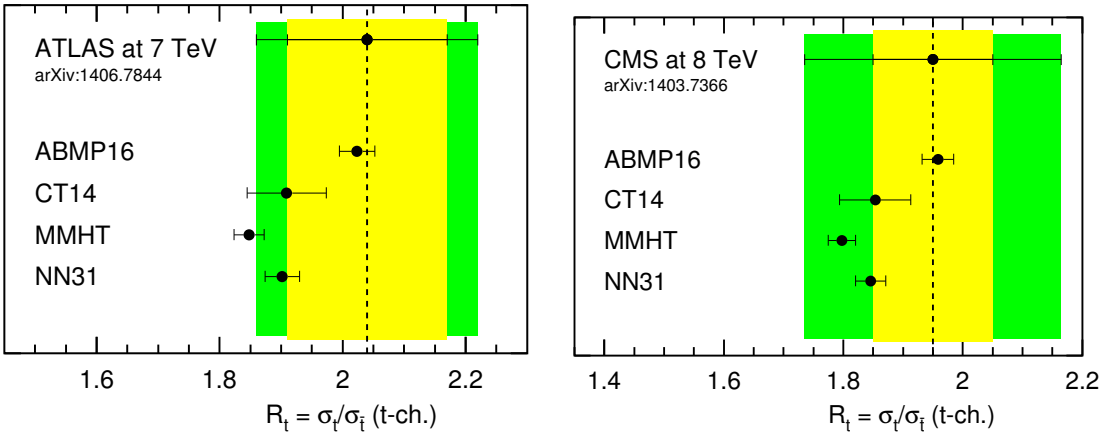

Figure 4: Same as in Figs. 2 and 3 for the ratio of cross sections $R_t = \sigma_{pp\to\bar{t}}/\sigma_{pp\to\bar{t}}$ in comparison to ATLAS data [11] at $\sqrt{s} = 7$ TeV (left) and to CMS data [12] at $\sqrt{s} = 8$ TeV (right).

To that end, it is important to keep in mind that quark masses are not physical observables, so that the determination of m_t relies on comparing the parametric dependence of the theory prediction $\sigma_{\rm th}(m_t)$ with the experimentally measured cross section value $\sigma_{\rm exp}$. The accuracy of the extracted top-quark mass is intrinsically limited by the sensitivity $\mathcal{S}$ of $\sigma_{\rm th}(m_t)$ to m_t,

$$\left|\frac{\Delta\sigma}{\sigma}\right| = \mathcal{S} \times \left|\frac{\Delta m_t}{m_t}\right| . \tag{2}$$

For the processes under consideration the sensitivity $\mathcal{S} \simeq 5$ for $t\bar{t}$ hadro-production and $\mathcal{S} \simeq 1.5$ for single-top production in the t-channel [10].

Next, the theory computation for $\sigma_{\rm th}(m_t)$ is performed at a given order in perturbation theory and requires the choice of a renormalization scheme for m_t. The most common choice are the on-shell scheme with the pole mass $m_t^{\rm pole}$ and the $\overline{\rm MS}$ scheme with the running top-quark mass $m_t(\mu_r)$, which are then extracted at a given order in perturbation theory. The different mass definition can be related to each other in perturbation theory, see, e.g., Ref. [18] and Ref. [19] for a review of relations between these and other renormalization schemes such as the so-called MSR mass.

Finally, it is important to address the correlation of the m_t dependence in $\sigma_{\rm th}(m_t)$ with all other input parameters, most prominently the PDFs in the proton and the strong coupling constant α_s. To account for those correlations any extraction of m_t from hadro-production cross sections should be performed as a global fit of m_t, the PDFs and α_s simultaneously [1]. Shifts in m_t for a given choice of a fixed value of α_s in variants of the global fit performed in Ref. [1] are illustrated in Fig. 5. As can be seen, these are sizable and easily exceed the experimental uncertainty on m_t indicated by the vertical bars.

Using the theory predictions with a running top-quark mass $m_t(\mu_r)$ at NNLO for $t\bar{t}$ production [20] and for single-top production [16] the global analysis of Ref. [1] determines n the $\overline{\rm MS}$ scheme at NNLO the value

$$m_t(m_t) \quad = \quad 160.9 \pm 1.1 \ \text{GeV} . \tag{3}$$

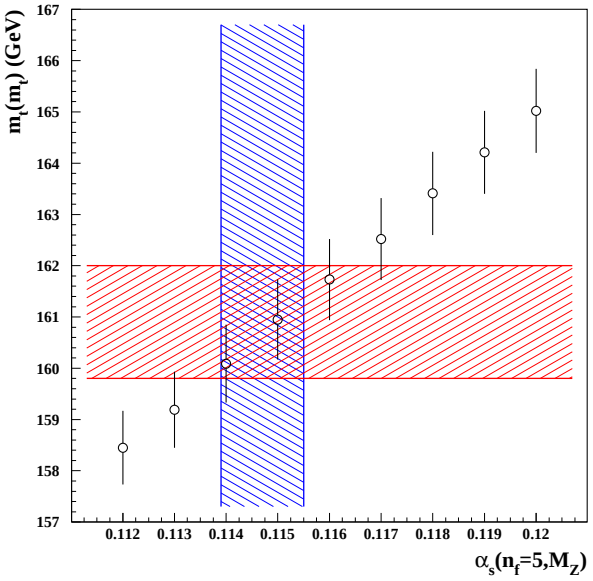

Figure 5: The $\overline{\rm MS}$ value of $m_t(m_t)$ obtained in the variants of the ABMP16 analysis with the value of $\alpha_s^{(n_f=5)}(M_Z)$ fixed in comparison with the 1σ bands for $m_t(m_t)$ and $\alpha_s^{(n_f=5)}(M_Z)$ obtained in the nominal ABMP16 fit (left-tilted and right-tilted hatch, respectively). Reprinted figure with permission from Ref. [1]. Copyright (2017) by the American Physical Society.

The top-quark mass in Eq. (3) has been extracted in a well-defined renormalization scheme with direct relation to the parameter in the QCD Lagrangian. A commonly used experimental procedure, on the other hand, performs a fit of the top-quark mass parameter used in Monte Carlo simulations of events with top-quark decays, when comparing those simulations to the kinematic measurement of the top-quark decay products. The mass determined in this way is therefore often referred to as the so-called top-quark Monte Carlo mass and the calibration of this mass parameter has been a long-standing problem, since no renormalization schemes has been specified in those Monte Carlo event generators.

To overcome this problem, Ref. [21] has proposed a method to establish experimentally the relation between the top-quark mass $m_t^{\rm MC}$ as implemented in a given Monte-Carlo generator and the Lagrangian mass parameter m_t in a theoretically well-defined renormalization scheme. The method proceeds through a simultaneous fit of $m_t^{\rm MC}$ and an observable with sensitivity to m_t, such as the inclusive $t\bar{t}$ cross section $\sigma_{pp\to t\bar{t}}$ discussed above. In particular, this approach does not rely on any prior assumptions about the relation between m_t and $m_t^{\rm MC}$, since the measured observable, e.g., $\sigma_{pp\to t\bar{t}}$ is independent of $m_t^{\rm MC}$ and can be used subsequently for a determination of m_t.

In Fig.6 the analysis strategy has been illustrated with a two parameter likelihood fit for the measured Monte Carlo mass $m_t^{\rm MC}$ and the inclusive $t\bar{t}$ production cross section $\sigma_{pp\to t\bar{t}}$. Using the measured value for $\sigma_{pp\to t\bar{t}}$ it is the possible to extract, e.g., the pole mass $m_t^{\rm pole}$ in a subsequent step and to determine the off-set $\Delta_m = m_t^{\rm pole} - m_t^{\rm MC}$. Examples from inclusive

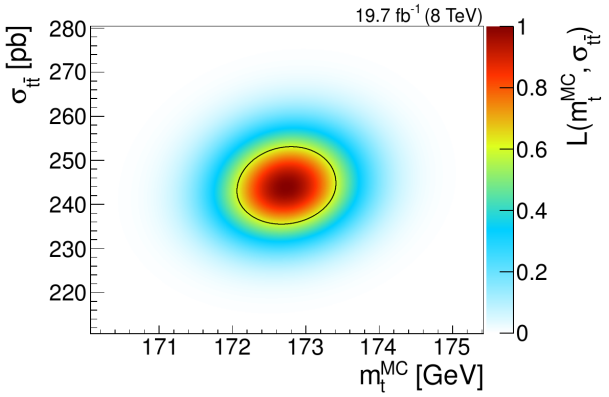

Figure 6: Likelihood L for the measured Monte Carlo mass m_t^{MC} and the $t\bar{t}$ production cross section $\sigma_{pp\to t\bar{t}}$ at a center-of-mass energy of $\sqrt{s} = 8$ TeV with the 1σ uncertainty denoted by the black contour. Reprinted figure with permission from Ref. [21]. Copyright (2016) by the American Physical Society.

and differential cross sections for hadro-production of top-quarks considered in Ref. [21] have led to $\Delta_m \simeq \mathcal{O}(2)$ GeV, depending on details of the analysis, of course.

2.3 Stability of the electroweak vacuum

In the light of the recent high-precision measurements of the Higgs boson mass $m_H = 125.09 \pm 0.24$ GeV [22], the measured values for the strong coupling α_s and the top-quark mass m_t, i.e., the Yukawa coupling of the top-quark to the Higgs boson give rise to an intriguing coincidence. The scalar potential $V(\phi)$ of the Higgs boson field ϕ, given by

$$V(\phi) = -\frac{m_\phi^2}{2}\phi^\dagger\phi + \lambda(\phi^\dagger\phi)^2\,, \tag{4}$$

is controlled by the scalar self-coupling $\lambda(\mu_r)$ and the quadratic Higgs mass parameter proportional to m_ϕ with the normalization $m_\phi = m_H$ at tree level, which combine in the expectation value of the electroweak vacuum as $v(\mu_r) = \sqrt{m_\phi^2(\mu_r)/(2\lambda(\mu_r))}$. It is possible for the Higgs potential to develop a second minimum at field values as large as the Planck scale $M_{Pl} \simeq 10^{19}$ GeV in addition to $v = 246$ GeV in which we live.

Investigations of the stability of the electroweak vacuum are therefore important to answer the question, if the SM can be extended to very high scales, where unification with gravity is expected. Requiring $\lambda(\mu_r) \geq 0$ at all scales up to the Planck scale M_{Pl} allows to formulate the condition for the vacuum stability as a lower bound on the mass of the Higgs boson as follows [23]

$$\begin{aligned} m_H \;=\; & 129.6\ \text{GeV} \\ & +1.8 \times \left(\frac{m_t^{\text{pole}} - 173.34\ \text{GeV}}{0.9}\right) - 0.5 \times \left(\frac{\alpha_s^{(n_f=5)}(M_Z) - 0.1184}{0.0007}\right)\ \text{GeV} \pm 0.3\ \text{GeV}\,, \end{aligned} \tag{5}$$

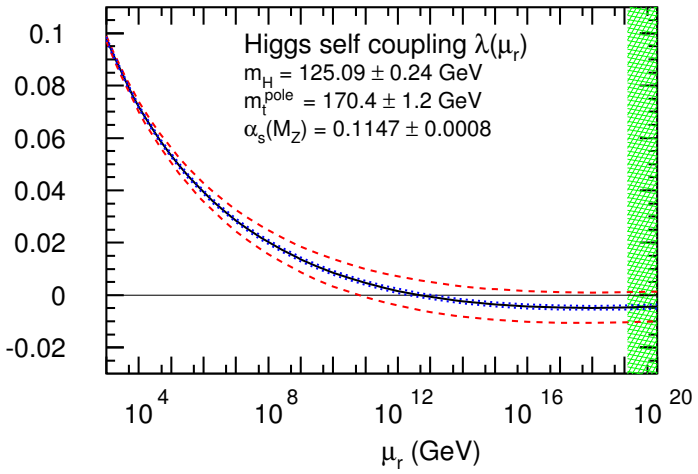

Figure 7: The renormalization group evolution of the Higgs boson self-coupling λ as a function of scale μ_r. The dashed (red) lines denote the combined 1σ uncertainty for $\alpha_s^{(n_f=5)}(M_Z)$ and $m_t^{\rm pole}$ and the dotted (blue) lines the 1σ uncertainty in the value of $m_H = 125.09 \pm 0.24$. The range of scales $\mu_r \geq M_{Pl}$ is indicated by the hatched (green) band on the right. Reprinted figure with permission from Ref. [1]. Copyright (2017) by the American Physical Society.

where m_t and α_s are to be taken in the on-shell and $\overline{\rm MS}$ schemes, respectively, and the uncertainty of $\pm 0.3\,$GeV appears due to missing higher-order corrections (see also Ref. [24]).

With the values determined in Ref. [1] at NNLO in QCD for the strong coupling, $\alpha_s^{(n_f=5)}(M_Z) = 0.1147 \pm 0.0008$ and the running top-quark mass $m_t(m_t)$, cf. Eq. (3), we are in a position to update previous work [25]. The value of m_t in Eq. (3) correspond to the pole mass $m_t^{\rm pole} = 170.4 \pm 1.2$ GeV at NNLO so that Eq. (5) leads to the bound

$$m_H \;=\; 126.3 \pm 2.5 \;\; \text{GeV}\,, \tag{6}$$

where all uncertainties have been added in quadrature. Thus, within its 1σ uncertainty this lower bound is compatible with the measured value $m_H = 125.09 \pm 0.24$ GeV [22] for the Higgs boson mass, allowing for stability up to the scale M_{Pl}.

In a complementary way this is illustrated in Fig. 7 showing the running of the Higgs boson self-coupling $\lambda(\mu_r)$ in full three-loop accuracy and with α_s and m_t obtained in Ref. [1] as the input parameters. The computation has been performed with the code `mr`, which implements matching and running of the SM parameters [26]. Clearly, a vanishing Higgs self-coupling $\lambda = 0$ at M_{Pl} remains a scenario which is compatible with the current values of α_s, m_t and m_H within their 1σ uncertainties. In addition, as follows from our analysis the value of $\lambda(\mu_r)$ remains strictly positive up to scales $\mu_r \sim \mathcal{O}(10^{12}\,\text{GeV})$, so that no new physics needs to be invoked in order to stabilize the electroweak vacuum.

2.4 Beyond the SM top-quark physics

Most models beyond the Standard Model treat the top-quark special as it is the heaviest known particle and couples most strongly to the electroweak symmetry breaking sector. We

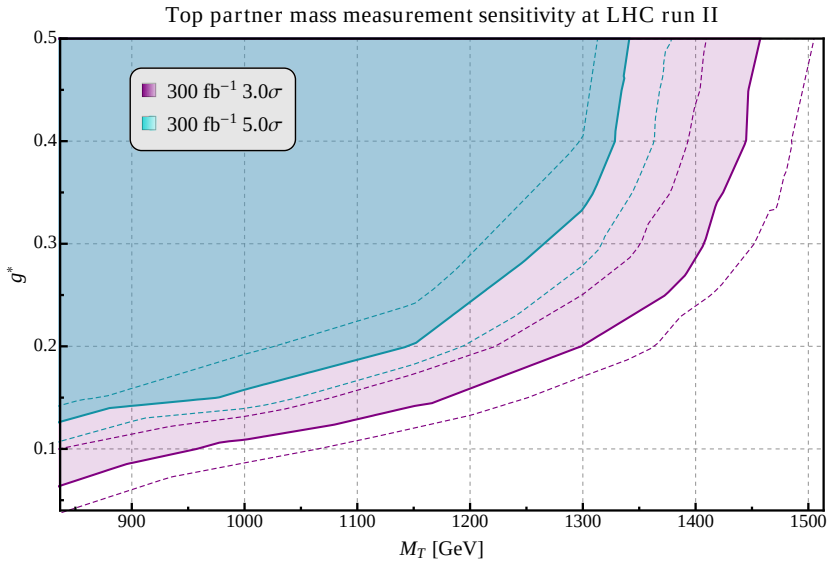

Figure 8: Sensitivity to top-partners at LHC Run 2 with $\sqrt{s} = 13$ TeV and 300 fb^{-1} of integrated luminosity using the $T \to tZ$ channel with hadronic boosted top reconstruction. Figure taken from Ref. [27].

just discuss here one particular aspect of new physics in the top-sector, namely the search for so-called heavy top-partners at the LHC and the possible measurements of their properties. These particles are predicted in many models to compensate the large radiative corrections to the Higgs potential from the SM top-quark. We focus here on fermionic top partners (denoted here as T), where searches in specific decay channels of these particles into the SM top-quark and a Z-boson, i.e., the decay $T \to tZ$, have been studied [27]. This channel has been studied for hadronically decaying top-quarks by means of so-called boosted top tagging techniques. As there is a huge mass gap expected between the top-partner and the SM top-quark, the SM top-quark gets a considerable boost which allows it to be treated with jet substructure techniques. Due to the leptonically decaying Z boson, this channel allows to fully reconstruct the mass of the top-partner particle in case of a discovery.

This has been studied in the context of simplified models, where only the top-partner and its electroweak and QCD couplings to SM particles are considered. Typical scenarios for such top-partners are models with composite Higgs boson or Little Higgs models, which have also been studied specifically in this context, cf. [28–30].

Possible discoveries of a top-partner have been quantified as a function of its mass and its universal electroweak coupling g^*. The sensitivity curves for 3σ evidence as well as for 5σ discovery are shown in Fig. 8. The shown bands include a possible additional non-statistical uncertainty of 30% on the visible cross section of the involved processes, e.g., from the experimental systematics in detection efficiencies. If a signal peak is observed, a measurement of the top-partner's invariant mass is possible with a resolution of $\Delta m_T = \pm 75$ GeV around the peak, at worst.

Another project focusing on new physics in the top-quark sector studied single-top production at the LHC as a means to measure possible anomalous charged-current contact interactions

in the top-quark sector [31]. This relies on an effective-field theory approach which parameterizes the effect of new physics in a model-independent way in the form of higher-dimensional four-fermion operators for $tbff'$ contact interactions whose Wilson coefficients can be interpreted as anomalous top-quark couplings. Here, binned likelihood distributions over specific kinematic observables have been studied to gain sensitivity on the Wilson coefficients. As a result it was found that for new physics scale $\Lambda_{\rm np}$ of $\Lambda_{\rm np} = 3$ TeV the LHC with $\sqrt{s} = 14$ TeV and 100 fb^{-1} integrated luminosity reaches a sensitivity of the order $\mathcal{O}(0.01-1)$ for the Wilson coefficients. Angular distributions can serve as spin analyzers for the top-quark and allow to resolve ambiguities in the parameter determination.

3 Top-quark physics at the ILC and CLIC

Top-quark physics represents together with Higgs boson precision measurements and the search for new physics one of the three cornerstones of the physics program of any future electron-positron collider. The ILC baseline design [32, 33] contains runs at center-of-mass energies of both $\sqrt{s} = 350$ GeV and 500 GeV, respectively, while the baseline design of the Compact Linear Collider (CLIC) [34, 35] contains stages at $\sqrt{s} = 380$ GeV, 1.4 TeV and 3 TeV, respectively. The new staging scenario foresees a long run of the ILC at $\sqrt{s} = 250$ GeV before an energy upgrade [36] containing the top-quark physics program. The work carried out for this top-quark physics program within this project encompasses fixed-order NLO QCD corrections for the fully off-shell leptonic top-decays, without and with an additional Higgs boson in the final state, i.e., the processes

$$e^+e^- \to e^+\nu_e\mu^-\bar{\nu}_\mu b\bar{b}(+H)\,, \tag{7}$$

see [37], as well as the matching of the fully exclusive resummed non-relativistic threshold corrections within non-relativistic QCD (NRQCD) at next-to-leading logarithmic accuracy (NLL) to the above mentioned continuum (NLO QCD) calculation [38]. Both calculations have been relying on the framework for automated NLO QCD calculations within the Monte-Carlo event generator `WHIZARD` [39] which has been developed during the final phase of the SFB 676.

In Ref. [37], top-pair production and top-pair production in association with a Higgs boson have been calculated at three different levels of off-shellness. First, for the on-shell processes,

$$e^+e^- \to t\bar{t}(H)\,, \tag{8}$$

second, with decaying top-quarks,

$$e^+e^- \to W^-bW^+\bar{b}(H)\,, \tag{9}$$

and, third, with leptonic W-boson decays,

$$e^+e^- \to e^+\nu_e\mu^-n\bar{u}_\mu b\bar{b}(H)\,. \tag{10}$$

For top-pair production, the main results are shown in Fig. 9. The left panel shows the total cross section at LO and NLO QCD for the full energy range up to the maximal energy of the CLIC project of $\sqrt{s} = 3$ TeV. The two panels at the bottom show the K-factor (the ratio between NLO and LO total sections), as well as the ratio of the off-shell to the on-shell process. This ratio is rising from unity close to threshold up to a factor of two, demonstrating that the non-resonant irreducible background becomes more and more important at higher energy.

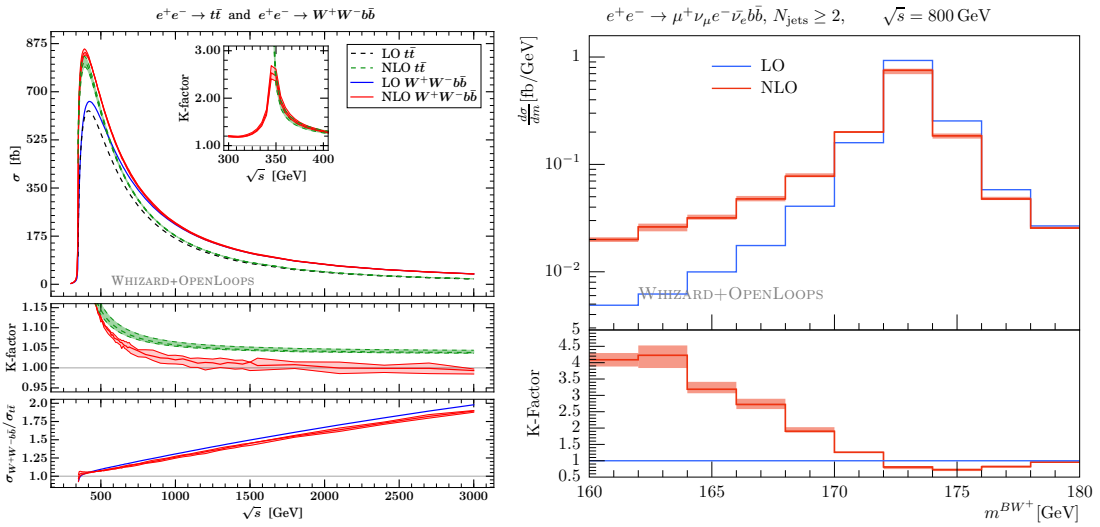

Figure 9: Left panel: Total cross section for $e^+e^- \to W^+bW^-\bar{b}$ at leading order (LO) QCD (blue) and NLO QCD (red), respectively. Dashed curves show the on-shell process $e^+e^- \to t\bar{t}$. The ratio plots show the K-factor (NLO QCD over LO QCD) and the off-shell over the on-shell process. The inset shows the K-factor close to threshold. Right panel: Differential distribution for the invariant mass of the b-jet and the W^+ for $e^+e^- \to e^+\nu_e\mu^-\bar{\nu}_\mu b\bar{b}$ at LO QCD (blue) and NLO QCD (red), respectively. The red band shows the scale uncertainties for $m_t/2 < \mu < 2m_t$ around the central scale $\mu = m_t$. Figures taken from Ref. [37].

The inset shows the K-factor in the proximity of the top-quark threshold, where fixed-order perturbation theory is not a good approximation any more due to the strong QCD binding effects of the non-relativistic top-quark pair. The right panel shows the differential distribution of the invariant mass of the b-jet and the W^+ at LO and NLO QCD, with the K-factor being clearly not constant over the phase space. In Fig. 10, the corresponding total cross section for off-shell top pair production in association with a Higgs boson is shown in the left panel. All curves have the corresponding meaning compared to Fig. 9. The right panel shows the total cross section for the off-shell process

$$e^+e^- \to W^+bW^-\bar{b}H\,, \tag{11}$$

as a function of the signal strength modifier $\xi_t = y_t/y_t^{SM}$ for the top-Yukawa coupling. It shows that the dependence on this modifier differs between LO and NLO QCD. The results from this NLO QCD calculation have been used by the CLICdp collaboration for the assessment on the precision with which the top-Yukawa coupling can be measured at CLIC for 1.4 TeV center-of-mass energy [40].

The most precise method known to measure the top-quark mass with an ultimate precision of $\Delta m_t = 30 - 70$ MeV is a template fit of the top threshold scan for the total inclusive cross section. The main uncertainties in addition to the unknown higher order corrections beyond next-to-next-to-next-to-leading order (NNNLO) in QCD are theoretical background uncertainties, systematic uncertainties due to selection efficiencies and uncertainties from the

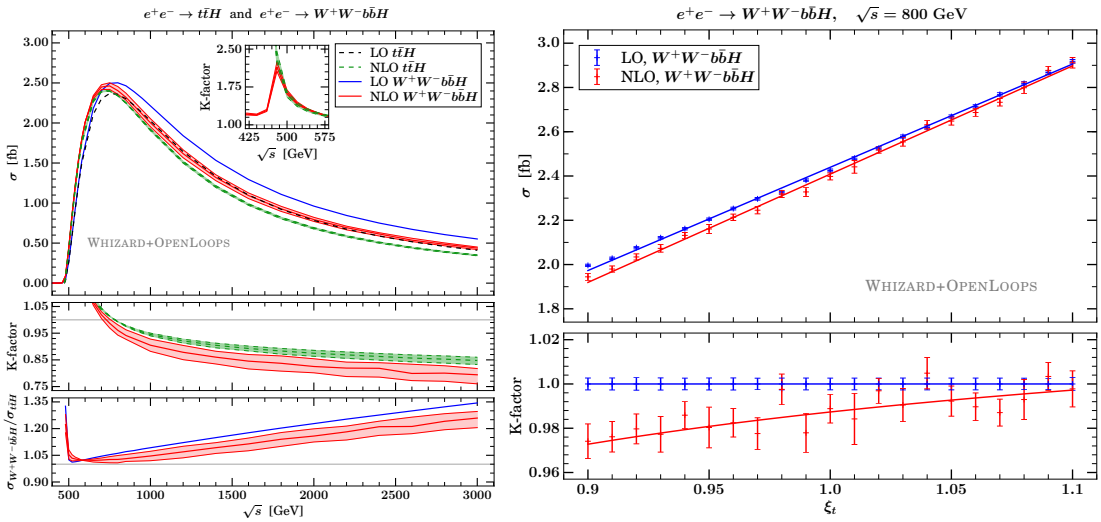

Figure 10: Left panel: Total cross section for $e^+e^- \to W^+bW^-\bar{b}H$ at LO QCD (blue) and NLO QCD (red), respectively. Dashed curves show the on-shell process $e^+e^- \to t\bar{t}H$. The ratio plots show the K-factor (NLO QCD over LO QCD) and the off-shell over the on-shell process. The inset shows the K-factor close to threshold. Right panel: Dependence of the total cross section for $e^+e^- \to W^+bW^-\bar{b}H$ at LO QCD (blue) and NLO QCD (red), respectively, on the signal strength modifier for the top-Yukawa coupling, $\xi_t = y_t/y_t^{SM}$. Figures taken from Ref. [37].

beam spectrum. All of the last three ones can be addressed with the work from [38]. The main difficulty is to properly match the non-relativistic effective-field theory calculation using NRQCD that is best suited right at the threshold with the relativistic NLO QCD calculation at the continuum. For that purpose, a factorized calculation in double-pole approximation with on-shell projection has been devised in [38] to subtract the double-counting of α_s corrections from both approaches, thereby maintaining full electroweak gauge invariance. The left panel of Fig. 11 shows the fully exclusive matched threshold scan for the process

$$e^+e^- \to W^+bW^-\bar{b}\,. \tag{12}$$

The blue curve shows the fixed-order NLO QCD calculation including scale variations, while the red curve shows the fully matched calculation. The red band includes uncertainties from the soft and hard NRQCD scale variations, the relativistic NLO QCD scale variations, variations over the details of the switch-off of the non-relativistic contributions in the continuum. (The dashed black line shows how the non-relativistic threshold calculation fails to describe top pair production properly in the continuum.) To be more conservative, scale variations are also symmetrized with respect to the central value line as the NRQCD scale variations are highly asymmetric. The plot includes the effects from an all-order resummation of soft-collinear QED photons from initial-state radiation as well as hard-collinear photons up to third order in α. The matched exclusive calculation provided in [38] allows for the first time to study differential top-quark distributions in the vicinity of the top threshold. This is shown in the right panel of Fig. 11 for the invariant mass of the b-jet and the W^+ boson. The blue curve shows the NLO QCD result, while the red curve shows the matched calculation.

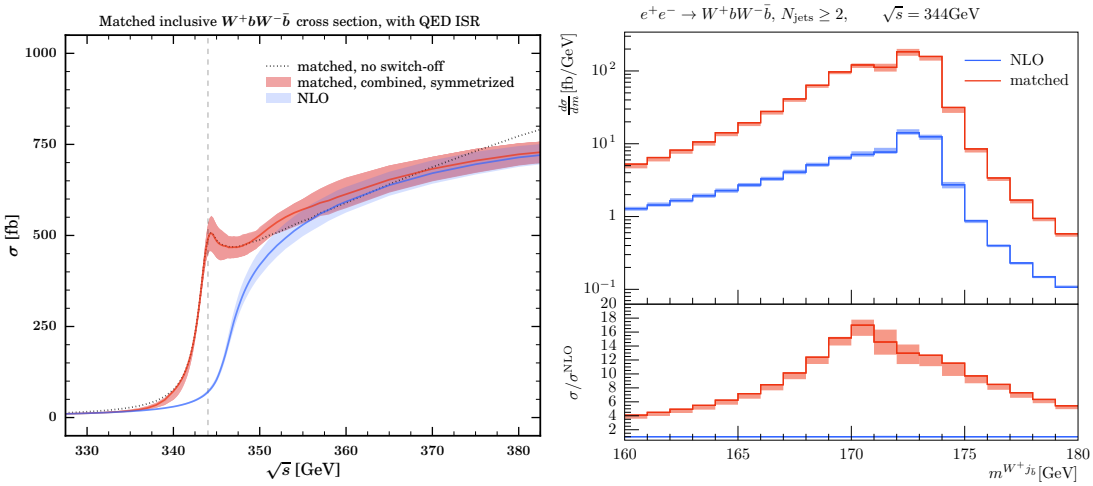

Figure 11: Left panel: Threshold scan for the exclusive process $e^+e^- \to W^+bW^-\bar{b}$ matched at NLL NRQCD (threshold) to NLO QCD (continuum), including full all-order QED initial state radiation effects. Right panel: Differential distribution for the invariant mass of the b-jet and the $W+$ boson at fixed order NLO QCD (blue) and fully matched (red), respectively. Figures taken from Ref. [38].

4 Conclusions

Top-quark physics is one the major fields in particle physics, both to study the properties of the heaviest known particle in Nature, as well as using it as a means to search for new physics. In this project, forefront precision calculations have been performed for the studies of the properties of the top-quark at the running LHC as well as for future lepton colliders. The calculations made in this project are very important for the measurement of the mass of the top-quark, the strong coupling constant, the top-Yukawa coupling and the width of the top-quark, as well as for a better understanding of the parton distribution functions of the proton. In addition, top-quark physics has been used as a tool for searches for new physics, e.g. for the search of heavy top-like new quarks, so-called top-partner particles.

Acknowledgments

S. M. gratefully acknowledges collaborations with S. Alekhin, J. Blümlein, J. Kieseler, K. Lipka, R. Placakyte and S. Thier; and J. R. R. wants to thank for collaborations with A.H. Hoang, W. Kilian, J. Lindert and S. Pozzorini.

References

[1] S. Alekhin, J. Blümlein, S. Moch and R. Placakyte, *Parton distribution functions, α_s, and heavy-quark masses for LHC Run II*, *Phys. Rev.* **D96** (2017) 014011, [1701.05838].

[2] P. Bärnreuther, M. Czakon and A. Mitov, *Percent Level Precision Physics at the Tevatron: First Genuine NNLO QCD Corrections to $q\bar{q} \to t\bar{t} + X$*, *Phys. Rev. Lett.* **109** (2012) 132001, [1204.5201].

[3] M. Czakon and A. Mitov, *NNLO corrections to top-pair production at hadron colliders: the all-fermionic scattering channels*, *JHEP* **12** (2012) 054, [1207.0236].

[4] M. Czakon and A. Mitov, *NNLO corrections to top pair production at hadron colliders: the quark-gluon reaction*, *JHEP* **01** (2013) 080, [1210.6832].

[5] M. Czakon, P. Fiedler and A. Mitov, *Total Top-Quark Pair-Production Cross Section at Hadron Colliders Through $O(\alpha_S^4)$*, *Phys. Rev. Lett.* **110** (2013) 252004, [1303.6254].

[6] M. Aliev, H. Lacker, U. Langenfeld, S. Moch, P. Uwer and M. Wiedermann, *HATHOR: HAdronic Top and Heavy quarks crOss section calculatoR*, *Comput. Phys. Commun.* **182** (2011) 1034–1046, [1007.1327].

[7] M. Brucherseifer, F. Caola and K. Melnikov, *On the NNLO QCD corrections to single-top production at the LHC*, *Phys. Lett.* **B736** (2014) 58–63, [1404.7116].

[8] E. L. Berger, J. Gao, C. P. Yuan and H. X. Zhu, *NNLO QCD Corrections to t-channel Single Top-Quark Production and Decay*, *Phys. Rev.* **D94** (2016) 071501, [1606.08463].

[9] S. Alekhin, J. Blümlein, S. Moch and R. Placakyte, *Isospin asymmetry of quark distributions and implications for single top-quark production at the LHC*, *Phys. Rev.* **D94** (2016) 114038, [1508.07923].

[10] P. Kant, O. M. Kind, T. Kintscher, T. Lohse, T. Martini, S. Mölbitz et al., *HatHor for single top-quark production: Updated predictions and uncertainty estimates for single top-quark production in hadronic collisions*, *Comput. Phys. Commun.* **191** (2015) 74–89, [1406.4403].

[11] ATLAS Collaboration, G. Aad et al., *Comprehensive measurements of t-channel single top-quark production cross sections at $\sqrt{s} = 7$ TeV with the ATLAS detector*, *Phys. Rev.* **D90** (2014) 112006, [1406.7844].

[12] CMS Collaboration, V. Khachatryan et al., *Measurement of the t-channel single-top-quark production cross section and of the $| V_{tb} |$ CKM matrix element in pp collisions at $\sqrt{s}$= 8 TeV*, *JHEP* **06** (2014) 090, [1403.7366].

[13] S. Dulat, T.-J. Hou, J. Gao, M. Guzzi, J. Huston, P. Nadolsky et al., *New parton distribution functions from a global analysis of quantum chromodynamics*, *Phys. Rev.* **D93** (2016) 033006, [1506.07443].

[14] L. A. Harland-Lang, A. D. Martin, P. Motylinski and R. S. Thorne, *Parton distributions in the LHC era: MMHT 2014 PDFs*, *Eur. Phys. J.* **C75** (2015) 204, [1412.3989].

[15] NNPDF Collaboration, R. D. Ball et al., *Parton distributions from high-precision collider data*, *Eur. Phys. J.* **C77** (2017) 663, [1706.00428].

[16] S. Alekhin, S. Moch and S. Thier, *Determination of the top-quark mass from hadro-production of single top-quarks*, *Phys. Lett.* **B763** (2016) 341–346, [1608.05212].

[17] S. Moch, *Precise heavy-quark masses*, *Nucl. Part. Phys. Proc.* **261-262** (2015) 130–139.

[18] P. Marquard, A. V. Smirnov, V. A. Smirnov, M. Steinhauser and D. Wellmann, *$\overline{\rm MS}$-on-shell quark mass relation up to four loops in QCD and a general SU(N) gauge group*, *Phys. Rev.* **D94** (2016) 074025, [1606.06754].

[19] S. Moch et al., *High precision fundamental constants at the TeV scale*, 1405.4781.

[20] U. Langenfeld, S. Moch and P. Uwer, *Measuring the running top-quark mass*, *Phys. Rev.* **D80** (2009) 054009, [0906.5273].

[21] J. Kieseler, K. Lipka and S.-O. Moch, *Calibration of the Top-Quark Monte Carlo Mass*, *Phys. Rev. Lett.* **116** (2016) 162001, [1511.00841].

[22] ATLAS, CMS Collaborations, G. Aad et al., *Combined Measurement of the Higgs Boson Mass in pp Collisions at $\sqrt{s} = 7$ and 8 TeV with the ATLAS and CMS Experiments*, *Phys. Rev. Lett.* **114** (2015) 191803, [1503.07589].

[23] D. Buttazzo, G. Degrassi, P. P. Giardino, G. F. Giudice, F. Sala, A. Salvio et al., *Investigating the near-criticality of the Higgs boson*, *JHEP* **12** (2013) 089, [1307.3536].

[24] A. V. Bednyakov, B. A. Kniehl, A. F. Pikelner and O. L. Veretin, *Stability of the Electroweak Vacuum: Gauge Independence and Advanced Precision*, *Phys. Rev. Lett.* **115** (2015) 201802, [1507.08833].

[25] S. Alekhin, A. Djouadi and S. Moch, *The top quark and Higgs boson masses and the stability of the electroweak vacuum*, *Phys. Lett.* **B716** (2012) 214–219, [1207.0980].

[26] B. A. Kniehl, A. F. Pikelner and O. L. Veretin, *mr: a C++ library for the matching and running of the Standard Model parameters*, *Comput. Phys. Commun.* **206** (2016) 84–96, [1601.08143].

[27] J. Reuter and M. Tonini, *Top Partner Discovery in the $T \to tZ$ channel at the LHC*, *JHEP* **01** (2015) 088, [1409.6962].

[28] J. Reuter and M. Tonini, *Can the 125 GeV Higgs be the Little Higgs?*, *JHEP* **02** (2013) 077, [1212.5930].

[29] J. Reuter, M. Tonini and M. de Vries, *Littlest Higgs with T-parity: Status and Prospects*, *JHEP* **02** (2014) 053, [1310.2918].

[30] D. Dercks, G. Moortgat-Pick, J. Reuter and S. Y. Shim, *The fate of the Littlest Higgs Model with T-parity under 13 TeV LHC Data*, *JHEP* **05** (2018) 049, [1801.06499].

[31] F. Bach and T. Ohl, *Anomalous top charged-current contact interactions in single top production at the LHC*, *Phys. Rev.* **D90** (2014) 074022, [1407.2546].

[32] H. Baer, T. Barklow, K. Fujii, Y. Gao, A. Hoang, S. Kanemura et al., *The International Linear Collider Technical Design Report - Volume 2: Physics*, 1306.6352.

[33] K. Fujii et al., *Physics Case for the International Linear Collider*, 1506.05992.

[34] L. Linssen, A. Miyamoto, M. Stanitzki and H. Weerts, *Physics and Detectors at CLIC: CLIC Conceptual Design Report*, 1202.5940.

[35] P. Lebrun, L. Linssen, A. Lucaci-Timoce, D. Schulte, F. Simon, S. Stapnes et al., *The CLIC Programme: Towards a Staged e+e- Linear Collider Exploring the Terascale : CLIC Conceptual Design Report*, 1209.2543.

[36] T. Barklow, J. Brau, K. Fujii, J. Gao, J. List, N. Walker et al., *ILC Operating Scenarios*, 1506.07830.

[37] B. Chokoufé Nejad, W. Kilian, J. M. Lindert, S. Pozzorini, J. Reuter and C. Weiss, *NLO QCD predictions for off-shell $t\bar{t}$ and $t\bar{t}H$ production and decay at a linear collider*, *JHEP* **12** (2016) 075, [1609.03390].

[38] F. Bach, B. C. Nejad, A. Hoang, W. Kilian, J. Reuter, M. Stahlhofen et al., *Fully-differential Top-Pair Production at a Lepton Collider: From Threshold to Continuum*, *JHEP* **03** (2018) 184, [1712.02220].

[39] W. Kilian, T. Ohl and J. Reuter, *WHIZARD: Simulating Multi-Particle Processes at LHC and ILC*, *Eur. Phys. J.* **C71** (2011) 1742, [0708.4233].

[40] CLICdp Collaboration, H. Abramowicz et al., *Top-Quark Physics at the CLIC Electron-Positron Linear Collider*, 1807.02441.